

Alongshore momentum balances in the nearshore

Falk Feddersen and R. T. Guza

Center for Coastal Studies, Scripps Institution of Oceanography, La Jolla, California

Steve Elgar

School of Electrical Engineering and Computer Science, Washington State University, Pullman

T. H. C. Herbers

Department of Oceanography, Naval Postgraduate School, Monterey, California

Abstract. The one-dimensional, time-averaged (over many wave periods) alongshore momentum balance between forcing by wind and breaking waves and the bottom stress is examined with field observations spanning a wide range of conditions on a barred beach. Near-bottom horizontal currents were measured for 2 months at 15 locations along a cross-shore transect extending 750 m from the shoreline to 8-m water depth. The hourly averaged bottom stress was estimated from observed currents using a quadratic drag law. The wave radiation stress was estimated in 8-m depth from an array of pressure sensors, and the wind stress was estimated from an anemometer at the seaward end of a nearby pier. The combined wind and wave forcing integrated over the entire cross-shore transect is balanced by the integrated bottom stress. The wind stress contributes about one third of the forcing over the transect. Analysis of the momentum balances in different cross-shore regions shows that in the surf zone, wave forcing is much larger than wind forcing and that the bottom drag coefficient is larger in the surf zone than farther seaward, consistent with earlier studies.

1. Introduction

Alongshore currents in the surf zone have been investigated extensively within the framework of steady, one-dimensional (1-D) models (*Bowen* [1969], *Longuet-Higgins* [1970], *Thornton* [1970], and others). If the topography, forcing, and alongshore current are steady and uniform in the alongshore direction, the time-averaged and vertically averaged alongshore momentum equation reduces to a 1-D balance between forcing, bottom stress, and mixing,

$$\tau_y^{\text{wind}} - \frac{\partial S_{yx}}{\partial x} = \tau_y^b + \frac{\partial F_{yx}}{\partial x} \quad (1)$$

where x and y are the cross-shore and alongshore coordinates, respectively. The forcing is the sum of the alongshore wind stress τ_y^{wind} , which although often ignored is sometimes important in the surf zone [*Whitford and Thornton*, 1993, 1996], and wave forcing, represented by the cross-shore gradient of the radiation stress component $-S_{yx}$ [*Longuet-Higgins and Stewart*, 1964]. Linear theory is used often to relate S_{yx} to the

frequency-directional wave spectrum $E(f, \theta)$ [e.g., *Battjes*, 1972] or in bulk wave transformation models to the wave height H_{rms} , mean wave angle $\bar{\theta}$, and the mean wave frequency \bar{f} [e.g., *Thornton and Guza*, 1983]. The mean alongshore bottom stress is often parameterized as [*Longuet-Higgins*, 1970]

$$\tau_y^b = \rho c_f \langle |\vec{u}|v \rangle \quad (2)$$

where ρ is the water density, c_f is a drag coefficient, $|\vec{u}|$ is the magnitude of the total velocity vector above the bottom boundary layer, v is the alongshore velocity component, and $\langle \rangle$ represents a time average over many wave periods. This quadratic form for the bottom stress has been used widely in steady channel flows [e.g., *Henderson*, 1966] but has not been verified directly in the surf zone. Mixing is given by the cross-shore gradient of the depth-integrated turbulent momentum flux F_{yx} . Although F_{yx} can be written exactly in terms of depth-integrated Reynolds stresses and the interaction of depth-varying currents [*Svendsen and Putrevu*, 1994], there is no accepted turbulence closure scheme, so F_{yx} is parameterized typically as proportional to the mean alongshore current shear $\partial \bar{v} / \partial x$, where \bar{v} is the time-averaged alongshore current.

The alongshore momentum equation (1) with the quadratic bottom stress (2) is difficult to solve for \bar{v} .

Copyright 1998 by the American Geophysical Union.

Paper number 98JC01270.
0148-0227/98/98JC-01270\$09.00

If a weak mean current and small wave angle are assumed, the bottom stress can be approximated as a linear function of \bar{v} [e.g., *Longuet-Higgins*, 1970]

$$\tau_y^b \propto \sigma_u \bar{v} \quad (3)$$

where σ_u^2 is the cross-shore orbital wave velocity variance. Given this approximation and parameterized forms for the wave transformation and mixing, solutions for \bar{v} can be found. However, in the surf zone the linearizing assumptions for the bottom stress often are violated [*Thornton and Guza*, 1986], and the general relationship between $\langle |\bar{u}|v \rangle$ and $\sigma_u \bar{v}$ is not understood well.

Alongshore currents predicted by (1) using a random wave transformation model for S_{yx} , a linearized bottom stress (3), and neglecting mixing ($\partial F_{yx}/\partial x = 0$) agree well with mean alongshore currents observed on a nearly plane beach with a small range of incident wave angles [*Thornton and Guza*, 1986]. However, there are large discrepancies between 1-D model predictions and observations on a barred beach near Duck, North Carolina acquired during the DELILAH field experiment [*Church and Thornton*, 1993; *Smith et al.*, 1993]. The beach at Duck is complex, with a wide range of wind and wave conditions [*Long*, 1996] and complicated bathymetry that includes prominent sandbars and sometimes pronounced alongshore inhomogeneities [*Lippmann and Holman*, 1990]. During DELILAH a broad alongshore current often was observed, with a single maximum shoreward of the crest of the sandbar, whereas 1-D models predict a flow with two narrow jets, one slightly seaward of the bar crest and one near the shoreline (i.e., in the regions where the predicted wave breaking causes large gradients in S_{yx}), with weak flow in between the jets.

The reasons for this discrepancy are unclear, but possible model deficiencies fall into two general classes. First, the 1-D momentum balance (1) may be correct, but the parameterization of wave forcing, bottom stress, or mixing may be either incorrect or not robust over the wide range of conditions at Duck (*Svendsen* [1984], *Church and Thornton* [1993], *Svendsen and Putrevu* [1994], *Dally and Brown* [1995], *Slinn et al.* [1998], *Garcez Faria et al.* [1998], and many others). Alternatively, the 1-D momentum balance (1) may be missing important two-dimensional (2-D) terms such as nonlinear advection and alongshore pressure gradients associated with alongshore depth variations. Model simulations suggest that these terms may be significant on natural beaches [*Putrevu et al.*, 1995; *Sancho et al.*, 1995; *Reniers et al.*, 1995].

Here the 1-D momentum balance (1) is tested with field observations (discussed in section 2) collected over a wide range of conditions on the barred beach near Duck, North Carolina. The alongshore momentum balance, integrated over the instrumented cross-shore transect, is examined in section 3. This integrated balance spanning the entire surf zone (as opposed to the local

balance examined by *Whitford and Thornton* [1996]) is independent of the poorly understood gradients of the turbulent momentum flux F_{yx} and radiation stress S_{yx} appearing in the local 1-D balance (1). The cross-shore integrated total (wind and wave) forcing is shown to be balanced approximately by the cross-shore integrated bottom stress, using the quadratic friction formulation (2). The closure of the cross-shore integrated momentum balance suggests that the dynamics of the alongshore current are on average described by the 1-D momentum balance (1). However, there are cases in which 2-D effects are important, as discussed in section 4. The results are summarized in section 5.

2. Observations

The data were collected during September and October of 1994 near Duck, North Carolina on a barrier island exposed to the Atlantic Ocean. The U.S. Army Corps of Engineers Field Research Facility (FRF) coordinate system, with x increasing offshore and y increasing in the northerly direction, is used. Directional properties of sea and swell were estimated from a two-dimensional array of 15 bottom-mounted pressure sensors in 8-m water depth (Figure 1), operated by the FRF [*Long*, 1996]. Hourly radiation stresses were estimated accurately using linear theory and a directional-moment-estimation technique that minimizes a weighted sum of the bias and statistical variability of the estimate [*Elgar et al.*, 1994]. Errors in the S_{yx} estimates are small compared to uncertainties in other terms of the integrated momentum balances investigated here. Wind speed and direction measured 19.5 m above mean sea level at the end of the nearby FRF pier were used

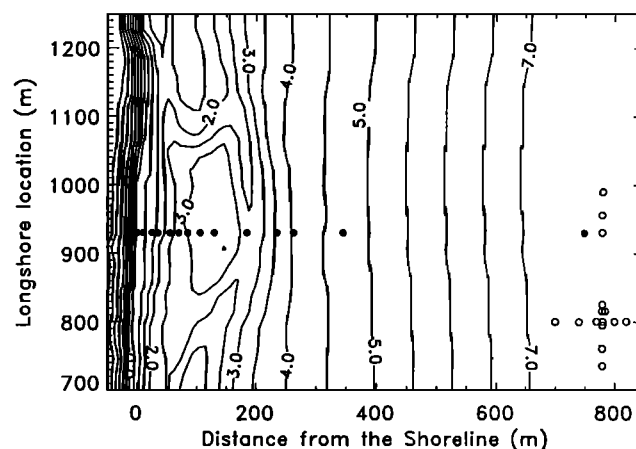


Figure 1. Plan view of the beach at Duck. A solid circle represents a colocated pressure sensor, current meter, and sonar altimeter. The open circles represent the Field Research Facility pressure sensor array. Bathymetry from October 20 is contoured in units of meters below mean sea level. Wind speed was measured about 500 m from the shoreline at alongshore location 500 m.

to estimate wind stress (S. Lentz, personal communication, 1995) using the algorithm of *Large and Pond* [1981]. No corrections were made for the possibly significant, but poorly understood, effect of waves on the wind stress [e.g., *Rieder et al.*, 1996]. Observations from a 60-km-long five-element alongshore array of pressure sensors in 6-m water depth [*Alessi et al.*, 1996] were used to obtain hourly estimates of the alongshore pressure gradient near the shore associated with shelf-scale barotropic motions (Appendix A).

Colocated sonar altimeters [*Gallagher et al.*, 1996], pressure sensors, and bidirectional electromagnetic current meters (sampled at 2 Hz) were deployed on a cross-shore transect extending 750 m from near the shoreline to 8-m water depth (Figures 1 and 2). Sonar altimeters measure acoustically the distance from the altimeter (mounted on a fixed frame) to the bed. Altimeter data were used to estimate depth profiles on the instrument transect [*Gallagher et al.*, 1998]. Current meter offset drift was accounted for by regularly rotating the current meters 180° and assuming a stationary mean current during approximately 10-min periods before and after the rotation. Biofouling required repeated cleaning of the current meter probes. Data from heavily biofouled current meters or with possibly large offset-drift-induced errors were discarded. Estimated errors in the measured mean alongshore flows are 0.05 m/s (arising primarily from offset drift) plus 5% of the true mean flow speed owing to inaccuracy in the current meter gain and orientation. The most nearshore sensor was often exposed at low tide and therefore inactive. The 15 current meters were raised or lowered as the bed level changed to maintain an elevation of 0.4–1.0 m above the seafloor.

Conditions during the experiment are summarized in Figure 3. In 8-m water depth the significant wave

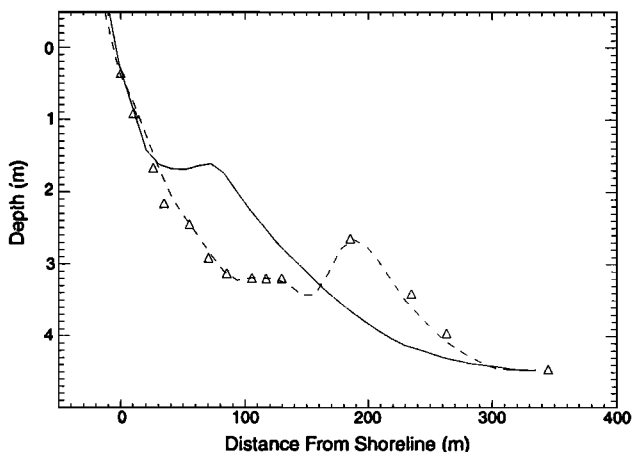


Figure 2. The cross-shore location of colocated current meters, pressure sensors, and sonar altimeters (triangles); bathymetry observed on August 25 (solid curve) and October 26 (dashed curve). An additional colocated pressure sensor and current meter in 8-m water depth, 750 m from the shoreline, is not shown.

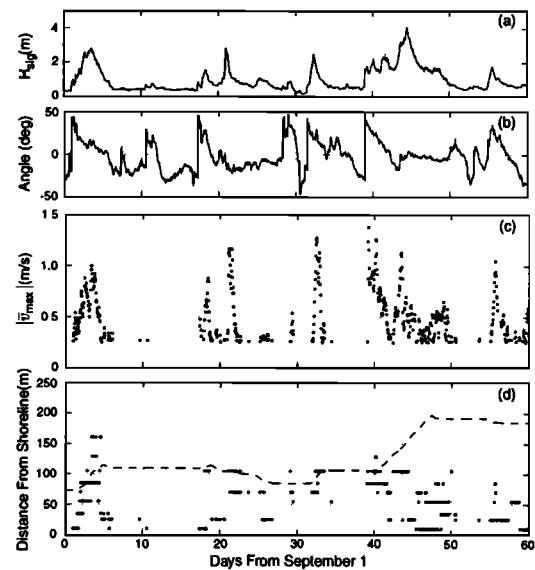


Figure 3. Hourly values of (a) significant wave height H_{sig} and (b) mean incident wave angle [*Kuik et al.* 1985] in 8-m depth (zero corresponds to normal incidence and positive angles to waves from the northern quadrant). (c) Absolute value of the maximum hourly averaged alongshore current $|\bar{v}_{max}|$ and (d) cross-shore location of the bar crest (dashed) and of \bar{v}_{max} . The 572 values of $|\bar{v}_{max}|$ shown correspond to hours with at least five active current meters and $|\bar{v}_{max}| \geq 0.25$ m/s. The few maxima occurring > 250 m from shore are not shown in Figure 3d.

height (H_{sig}) ranged between 0.2 and 4.0 m (Figure 3a), and the mean wave angle ranged between $\pm 50^\circ$ (Figure 3b). The mean (e.g., centroidal) wave frequency ranged between 0.08 and 0.2 Hz (not shown). The maximum mean alongshore current $|\bar{v}_{max}|$ (in each hour-long record) ranged from 0.1 to 1.4 m/s (Figure 3c). The bar crest, originally located 80 m from the shoreline, migrated 120 m farther offshore (Figure 3d and Figure 2). The observed locations of \bar{v}_{max} spanned the entire instrumented region, but were usually located within 150 m of the shoreline, and shoreward of the bar crest (Figure 3d). The few maxima located well seaward of the bar crest ($400 \text{ m} < x \leq 750 \text{ m}$) were weak ($|\bar{v}_{max}| \sim 0.3 - 0.4$ m/s) and approximately correspond to times of strong buoyancy-driven flows [*Rennie*, 1998]. The stronger alongshore currents ($|\bar{v}_{max}| \geq 0.8$ m/s) were often wave driven (e.g., associated with large S_{yx} in 8-m water depth, Figure 4) and occurred near the bar crest. Maxima near the shoreline were weaker (0.25–0.7 m/s). Many of the larger $|\bar{v}_{max}|$ (0.4–0.7 m/s) near the shoreline occurred in mid to late October after the sandbar migrated offshore (Figure 3d). The alongshore component of the wind ranged between 15 m/s from the north and 10 m/s from the south (not shown). The surf zone width (estimated as described in Appendix B) ranged from 10 to 750 m. Spring tides were about 1 m, and the slope of the beach foreshore was about 1/10 (Figure 2), so tidal fluctuations in the mean shoreline

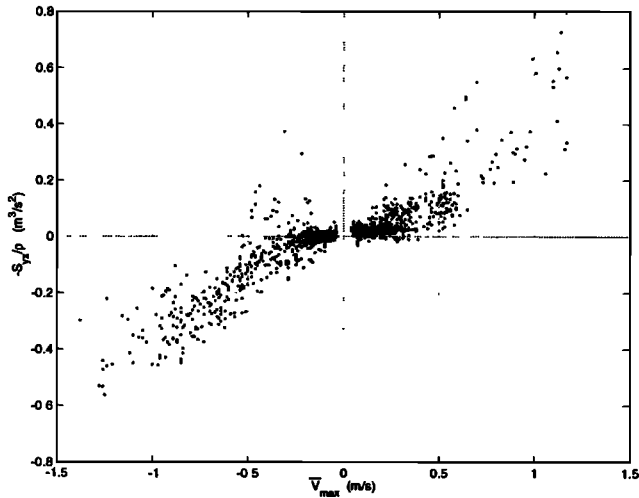


Figure 4. The radiation stress $-S_{yx}/\rho$ in 8-m depth versus the alongshore current maximum \bar{v}_{\max} ($r^2 = 0.76$). An observation is shown only if at least five sensors were active.

location were about 10 m. Alongshore barotropic tidal currents in water depths < 8 m were less than roughly 0.03 m/s (S. Lentz, personal communication, 1996).

Spatially extensive bathymetric surveys (e.g., Figure 1) were obtained several times during the data collection period with the CRAB (Coastal Research Amphibious Buggy). The orientations of the 1-, 2-, 3-, 4-, and 5-m depth contours over an alongshore span of 300 m that included the instrumented transect were determined by least squares fits of each depth contour to a straight line. The orientation angle of a particular depth contour changed over time, and the orientation of different depth contours varied $O(5^\circ)$ within a given survey. Particular depth contours sometimes were fit poorly by the surveys, indicating that the bathymetry was alongshore inhomogeneous (e.g., Figure 1). However, mean (averaged over all depths for a single survey) contour orientations varied by no more than $\pm 2^\circ$ from the FRF coordinate system. The results in section 3 are not altered significantly by $\pm 2^\circ$ rotation of the coordinate frame.

Guza *et al.* [1986] reported a strong correlation ($r^2 = 0.94$) between an empirical orthogonal function-derived \bar{v}_{\max} and $-S_{yx}$ estimated outside the surf zone on a nearly plane beach with a smaller range of incident wave angles than those observed here. The lower correlation between \bar{v}_{\max} and $-S_{yx}$ ($r^2 = 0.76$) at Duck (Figure 4) reflects a greater complexity of bathymetric, wave, and wind conditions. Wind stress, buoyancy forcing, the effect of alongshore inhomogeneities, and flow acceleration all contribute to the scatter between $-S_{yx}$ and \bar{v}_{\max} and dominate cases in which $-S_{yx}$ and \bar{v}_{\max} have opposite sign. The overall importance of terms other than S_{yx} to the alongshore momentum balance is unknown.

Wind is sometimes a substantial momentum source in the nearshore [Whitford and Thornton, 1993] and is

included in the momentum balances investigated here. The sometimes significant effect of wind forcing and the dynamical separation between the surf zone and the wind-driven region seaward of the surf zone is illustrated in Figure 5 for a case where wind and wave forcing have opposite sign. Moderately energetic waves ($H_{\text{sig}} \approx 1$ m in 8-m water depth) approached from the south while the 4 m/s wind was from the north. The wind-driven current flowed toward the south seaward of the bar crest, and a wave-driven current flowed toward the north shoreward of the bar crest (where wave breaking began). The observed sign change in \bar{v} highlights the transition from wind- to wave-driven flow. Even though the alongshore currents were weak, the division between the wind- and the wave-driven regimes was observable for the entire 48-hour period (September 20-21) when wind and wave forcing had opposite sign, and the location of current reversal fluctuated as the surf zone width was modulated by tidal changes in water depth. See Feddersen *et al.* [1996] for further discussion of case studies.

3. Alongshore Momentum Balances

The depth-integrated and time-averaged alongshore momentum equation is [e.g., Mei, 1989]

$$\rho(\bar{\eta} + h) \left(\frac{\partial \bar{v}}{\partial t} + \bar{u} \frac{\partial \bar{v}}{\partial x} + \bar{v} \frac{\partial \bar{v}}{\partial y} \right) = -\rho g(h + \bar{\eta}) \frac{\partial \bar{\eta}}{\partial y} - \frac{\partial S_{yx}}{\partial x} - \frac{\partial S_{yy}}{\partial y} - \tau_y^b + \tau_y^{\text{wind}} - \left(\frac{\partial F_{yx}}{\partial x} + \frac{\partial F_{yy}}{\partial y} \right) \quad (4)$$

where \bar{u} and \bar{v} are the depth- and time-averaged (over many wave cycles) cross-shore and alongshore velocities, h is the water depth, $\bar{\eta}$ is the mean free surface displacement, S_{yx} and S_{yy} are components of the radiation stress tensor, F_{yx} and F_{yy} are components of the depth-integrated turbulent momentum flux tensor, and τ_y^{wind} is the alongshore component of the wind stress. The alongshore bottom stress τ_y^b is represented by a

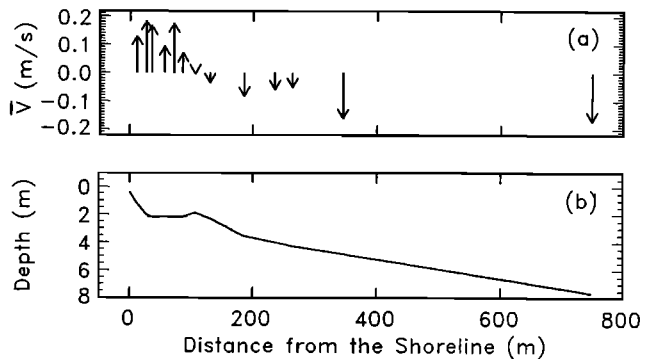


Figure 5. (a) Hourly averaged alongshore current \bar{v} versus distance from the shoreline and (b) depth observed at 1300 eastern standard time September 21. Arrows pointing toward the bottom of the figure indicate southward flow.

quadratic drag law (2). Earth rotation and variation of the water density ρ are neglected.

The assumptions of a steady state and no alongshore (y) variation, coupled with the continuity equation and a no mass flux boundary condition at the shoreline, yield $\bar{u} = 0$. The nonlinear terms and alongshore gradients of S_{yy} , F_{yy} , and $\bar{\eta}$ in (4) therefore vanish, and the alongshore momentum equation (4) simplifies to the one-dimensional balance (1).

The 1-D momentum balance (1) is not verified locally (e.g., at a single location) because gradients of the radiation stress S_{yx} and the turbulent momentum flux F_{yx} cannot be estimated well from these observations. However, if S_{yx} and F_{yx} are known at two cross-shore locations x_1 and x_2 , the cross-shore integral of (1) between x_1 and x_2 can be estimated as

$$\int_{x_1}^{x_2} \frac{\tau_y^{\text{wind}}}{\rho} dx - \frac{S_{yx}}{\rho} \Big|_{x_2} + \frac{S_{yx}}{\rho} \Big|_{x_1} = \int_{x_1}^{x_2} c_f \langle |\bar{u}|v \rangle dx + \frac{F_{yx}}{\rho} \Big|_{x_2} - \frac{F_{yx}}{\rho} \Big|_{x_1} \quad (5)$$

Here this integrated balance is tested statistically for several cross-shore regions. The spatial structure of the alongshore current is not addressed by the analysis.

The first integration region spans the entire 750-m-long transect, from near the shoreline ($x_1 = 0$) to 8-m water depth ($x_2 = x_{8m}$). Pressure array data in 8-m water depth are used to estimate S_{yx} at x_{8m} . The turbulent momentum flux F_{yx} is assumed negligible in 8-m water depth ($F_{yx}|_{x_{8m}} = 0$) because the surf zone (where mixing is believed strongest) rarely extended to x_{8m} . Assuming that S_{yx} and F_{yx} are zero at the shoreline and that c_f and τ_y^{wind} are spatially homogeneous, (5) becomes

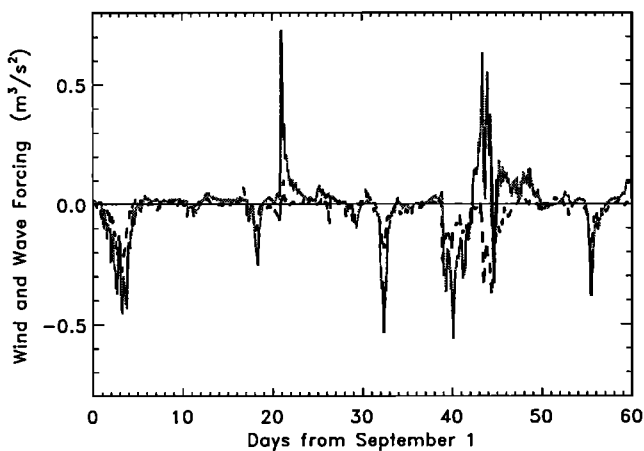


Figure 6. Hourly integrated (from the shoreline to 8-m depth) wave ($-S_{yx}/\rho|_{x_{8m}}$, solid curve) and wind ($\int_0^{x_{8m}} (\tau_y^{\text{wind}}/\rho) dx$, dashed curve) forcing versus time. Positive corresponds to northward forcing. The means are -0.0085 and $-0.0278 \text{ m}^3/\text{s}^2$, and the standard deviations are 0.1296 and $0.0616 \text{ m}^3/\text{s}^2$ for wave and wind forcing, respectively.

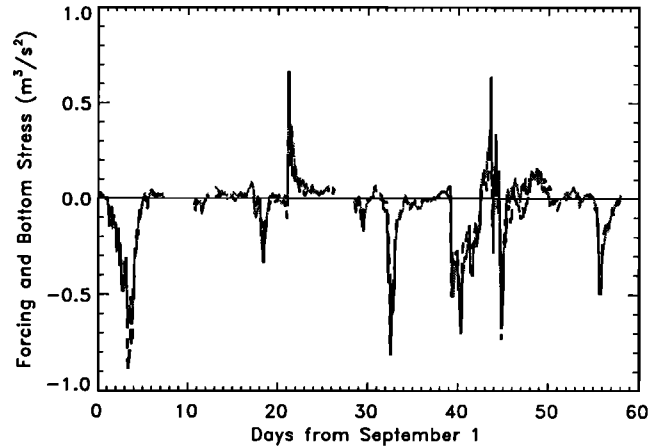


Figure 7. Hourly total forcing (wind and wave, $-S_{yx}/\rho|_{x_{8m}} + \int_0^{x_{8m}} (\tau_y^{\text{wind}}/\rho) dx$, solid curve) and bottom stress ($c_f \int_0^{x_{8m}} \langle |\bar{u}|v \rangle dx$, dashed curve) integrated from the shoreline to 8-m depth with a best fit $c_f = 0.0015$ versus time. Gaps occur when the bottom stress integral could not be computed because of inactive sensors. The correlation coefficient squared $r^2 = 0.87$.

$$\frac{\tau_y^{\text{wind}}}{\rho} x_{8m} - \frac{S_{yx}}{\rho} \Big|_{x_{8m}} = c_f \int_0^{x_{8m}} \langle |\bar{u}|v \rangle dx \quad (6)$$

where the only unknown is c_f . The integral is estimated from the observations as described in Appendix C.

Wind ($\tau_y^{\text{wind}} x_{8m}/\rho$) and wave ($-S_{yx}/\rho|_{x_{8m}}$) forcing terms integrated across the 750-m region during the 2-month experiment are shown in Figure 6. The rms wind forcing is about half the rms wave forcing and thus cannot be neglected. The wind and wave forcing are visually correlated but occasionally have opposite signs (e.g., September 20–21, days 19–20, and October 14, day 43, in Figure 6).

The integrated total (wind and wave) forcing and bottom stress are highly correlated ($r^2 = 0.87$), and linear regression gives a best fit $c_f = 0.0015 (\pm 1.2 \times 10^{-4})$, the 95% confidence limits on c_f (Figure 7). The linear relationship suggests that the current meter array adequately resolved the cross-shore structure of the flow, the bottom stress is represented well by (2), and the integrated 1-D momentum balance holds.

The integrated wind forcing is not negligible, but because the wind and wave forcing terms are correlated (Figure 6) it is possible that a balance between integrated wave forcing and bottom stress (i.e., neglecting wind forcing) closes equally well. However, the correlation between wave forcing and bottom stress ($r^2 = 0.73$) is significantly (at the 95% confidence level) lower than the correlation including wind forcing ($r^2 = 0.87$), demonstrating the importance of wind forcing over this region. The drag coefficient estimate is reduced from $c_f = 0.0015$, when wind stress is included, to $c_f = 0.0010$, when it is neglected.

To investigate possible spatial variation in c_f , the instrumented cross-shore transect was divided into regions within and seaward of the surf zone. Without assumptions about the evolution of S_{yx} and introducing friction coefficients c_{f1} and c_{f2} within and seaward of the surf zone, respectively, the momentum balances in each region are

$$\frac{\tau_y^{\text{wind}}}{\rho} x_b - \frac{S_{yx}}{\rho} \Big|_{x_b} = c_{f1} \int_0^{x_b} \langle |\bar{u}|v \rangle dx + \frac{F_{yx}}{\rho} \Big|_{x_b} \quad (7)$$

and

$$\begin{aligned} \frac{\tau_y^{\text{wind}}}{\rho} (x_{8m} - x_b) - \frac{S_{yx}}{\rho} \Big|_{x_{8m}} + \frac{S_{yx}}{\rho} \Big|_{x_b} \\ = c_{f2} \int_{x_b}^{x_{8m}} \langle |\bar{u}|v \rangle dx - \frac{F_{yx}}{\rho} \Big|_{x_b} \end{aligned} \quad (8)$$

where x_b is the location of the border between the two regions. Adding (7) and (8) yields a balance over the entire region similar to (6) (but with a variable drag coefficient) given by

$$\begin{aligned} \frac{\tau_y^{\text{wind}}}{\rho} x_{8m} - \frac{S_{yx}}{\rho} \Big|_{x_{8m}} = c_{f1} \int_0^{x_b} \langle |\bar{u}|v \rangle dx \\ + c_{f2} \int_{x_b}^{x_{8m}} \langle |\bar{u}|v \rangle dx \end{aligned} \quad (9)$$

The location of x_b is determined from estimated changes in wave energy flux as described in Appendix B. Only cases with several sensors both within and seaward of the surf zone are included (Appendix C) in determining, using multiple linear regression, best fit values for the drag coefficients. For the subset of data used to find c_{f1} and c_{f2} the correlation with a varying c_f ($r^2 = 0.82$) is significantly higher (at 95% confidence limits) than with a constant c_f ($r^2 = 0.76$). The regression yields $c_{f1} = 0.0033 (\pm 6.9 \times 10^{-4})$ and $c_{f2} = 0.0010 (\pm 2.3 \times 10^{-4})$.

The closure of the integrated-to-8-m-depth momentum balances (6) and (9) suggests that the quadratic form (2) does represent well the mean alongshore bottom stress. *Cox et al.* [1996] recently demonstrated in a laboratory surf zone that the instantaneous cross-shore bottom stress inferred from logarithmic oscillating boundary layer theory is related to the instantaneous product $|u|u$ outside the boundary layer over most phases of a wave cycle. The utility of the quadratic bottom stress parameterization is thus supported by observations at different temporal and spatial scales.

The surf zone drag coefficient $c_{f1} = 0.0033$ is similar to the c_f values inferred by *Whitford and Thornton* [1996] and (for low bed roughness) *Garcez Faria et al.* [1998]. The larger inferred c_f in the surf zone is consistent with the hypothesis that breaking-wave-induced turbulence enhances vertical mixing and thus

increases the bottom stress for the same free stream velocity [*Church and Thornton*, 1993] and is consistent with the magnitude of c_f variations observed by *Cox et al.* [1996].

Assuming S_{yx} is conserved seaward of x_b (e.g., $S_{yx}|_{x_b} = S_{yx}|_{x_{8m}}$) and the turbulent momentum flux at x_b is negligible (e.g., $F_{yx}|_{x_b} = 0$), the momentum balances within (7) and seaward (8) of the surf zone can be considered separately. In the surf zone the balance is between wind and wave forcing and bottom stress

$$\frac{\tau_y^{\text{wind}}}{\rho} x_b - \frac{S_{yx}}{\rho} \Big|_{x_{8m}} = c_{f1} \int_0^{x_b} \langle |\bar{u}|v \rangle dx \quad (10)$$

whereas seaward of x_b , the balance is between wind forcing and bottom stress

$$\frac{\tau_y^{\text{wind}}}{\rho} (x_{8m} - x_b) = c_{f2} \int_{x_b}^{x_{8m}} \langle |\bar{u}|v \rangle dx \quad (11)$$

For the surf zone momentum balance (10) $r^2 = 0.79$, and the best fit drag coefficient is $c_{f1} = 0.0035 (\pm 4.1 \times 10^{-4})$ (Figure 8). On average, the wind forcing is small, roughly 10% of the wave forcing in the surf zone (although in some cases, the wind stress is important). The similarity between the surf zone drag coefficients inferred from (10) and (9) suggests that the turbulent momentum flux across x_b , $F_{yx}|_{x_b}$ (neglected in (10)) is either uncorrelated with (which seems unlikely) or is small relative to the surf zone bottom stress.

The momentum balance (11) between wind forcing and bottom stress seaward of the surf zone ($r^2 = 0.36$, Figure 9) does not close as well as the surf zone momentum balance (10). If the errors causing the low correlation result solely from (Gaussian, zero mean) es-

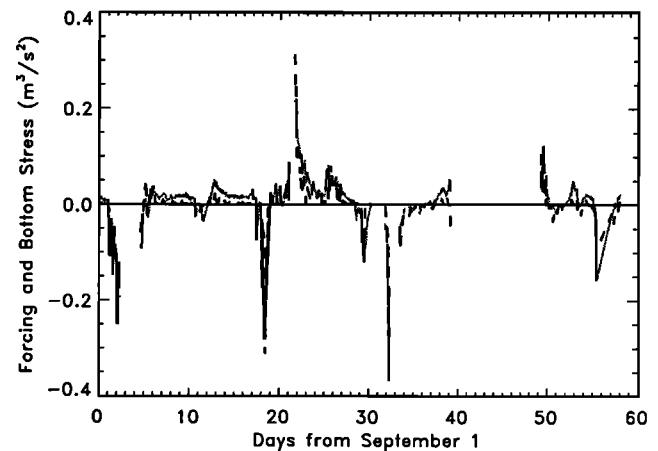


Figure 8. Hourly total forcing (wind and wave, $-S_{yx}/\rho|_{x_{8m}} + \int_0^{x_b} (\tau_y^{\text{wind}}/\rho) dx$, solid curve) and bottom stress ($c_{f1} \int_0^{x_b} \langle |\bar{u}|v \rangle dx$ with $c_{f1} = 0.0035$, dashed curve) integrated over the surf zone versus time. The correlation coefficient squared $r^2 = 0.79$.

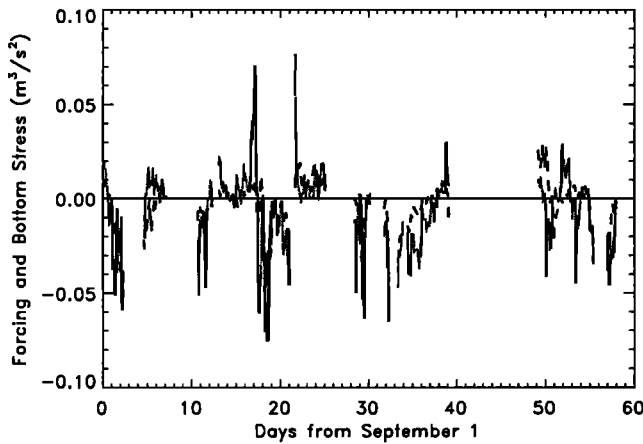


Figure 9. Hourly wind forcing ($\int_{x_b}^{x_{sm}} (\tau_y^{\text{wind}}/\rho) dx$, solid curve) and bottom stress ($c_{f2} \int_{x_b}^{x_{sm}} <|\bar{u}|v > dx$ with $c_{f2} = 0.00055$, dashed curve) integrated seaward of the surf zone versus time. The correlation coefficient squared $r^2 = 0.36$.

timation error of the wind forcing or bottom stress, the drag coefficient would be similar to the one estimated by (9). However, the drag coefficients are different. The reduced estimate of $c_f = 0.00055 (\pm 2.0 \times 10^{-4})$ from the seaward of the surf zone balance (11) versus $c_f = 0.0010 (\pm 2.3 \times 10^{-4})$ from (9) suggests that the balance (11) does not account for sources of momentum important to the region seaward of the surf zone, which are implicitly included in (9). For example, S_{yx} may not be conserved seaward of the estimated x_b . Alternatively, the turbulent momentum flux F_{yx} across x_b may be significant relative to the bottom stress seaward of the surf zone, and thus the surf zone may be a substantial source of momentum to the region seaward of the surf zone. The present observations cannot be used to separate these two possible sources of momentum.

4. Discussion

Other terms appearing in (4), but not in steady 1-D models (1), can be estimated in their integrated form with these data. The integration region extends to 8-m water depth, usually well seaward of the surf zone, and thus larger-scale inner shelf dynamics may be important over the instrument transect. For example, in 30-m water depth on the inner shelf of northern California, the alongshore barotropic pressure gradient (e.g., $-gh\partial\bar{\eta}/\partial y$) is an $O(1)$ term in the alongshore momentum balance [Lentz, 1994], and varies on alongshore length scales of $O(10\text{-}100\text{ km})$. These gradients were estimated here using observations in 6-m water depth [Alessi et al., 1996] as described in Appendix A. Assuming $\bar{\eta} \ll h$ and that $\partial\bar{\eta}/\partial y$ does not vary across the integration region, the cross-shore integral from shore to 8-m water depth of the pressure gradient is estimated as

$$-g \frac{\partial \bar{\eta}}{\partial y} \int_0^{x_{sm}} h dx$$

This barotropic pressure gradient is not dynamically important over the 750-m-long transect. It is usually a factor of 3 smaller than the wind forcing and is uncorrelated with any other dynamical terms. Alongshore baroclinic pressure gradients (not included in (4)) caused by Chesapeake Bay outflow can be significant on the inner shelf [Rennie, 1998] and might be important at times in the present momentum balances but cannot be quantified with this data set.

The integral of the acceleration term in (4) was also estimated. Using the continuity equation and assuming $\bar{\eta} \ll h$ and weak vertical variation of the alongshore current [Garcez Faria et al., 1998], the term $(\bar{\eta}+h)\partial\bar{v}/\partial t$ can be transformed to $\partial[h\bar{v}]/\partial t$. The acceleration, estimated by finite differencing the hourly transport

$$\int_0^{x_{sm}} h \bar{v} dx$$

is uncorrelated ($r^2 = -0.0018$) with and has one fifth the rms value of the total forcing. The lack of correlation with forcing suggests that the acceleration estimate is contaminated by noise, but the low rms values imply that the acceleration term is usually small. When the forcing changes rapidly (i.e., on September 21 in Figure 7) the hourly averaged flow responds within about an hour (e.g., the current lags the forcing by no more than 1 temporal sample). This rapid response to large changes in forcing further suggests that the alongshore current is nearly always in frictional balance and that flow accelerations are negligible.

The statistical analysis in section 3 demonstrates that the 1-D integrated momentum balance from the shoreline to 8-m water depth (6) closes, indicating that over the entire instrumented transect the combined wind and wave forcing is balanced by the bottom stress. The closure does not necessarily imply that the 1-D momentum balance (1) holds locally, because 2-D terms in (4) (e.g., nonlinear and alongshore pressure gradient) could be locally strong but change sign with cross-shore location such that their cross-shore integrals cancel. However, consistent cancellation seems unlikely to occur over the wide range of bathymetric and forcing conditions encountered during the 2-month experiment. Therefore the closure of the integrated momentum balance suggests that 2-D terms are typically small.

There are cases when the flow appears to be dominated by 2-D effects such as alongshore pressure gradients. For example, on October 16 (Figure 10) the waves were energetic ($H_{\text{sig}} = 3\text{ m}$ in 8-m water depth) but nearly normally incident (mean wave angle of 2°), so $-S_{yx}$ in 8-m water depth was small ($-0.023\text{ m}^3/\text{s}^2$). Wave breaking extended to 8-m water depth and was most intense about 150-200 m from shore (Figure 10a), well offshore of the strongest currents ($\bar{v}_{\text{max}} = -0.49\text{ m/s}$ near the shoreline, Figure 10b). In contrast to the observations, 1-D models predict weak currents everywhere ($|\bar{v}| \leq 0.05\text{ m/s}$) for the small wave angles observed. Time-elapsed video images (R.A. Holman,

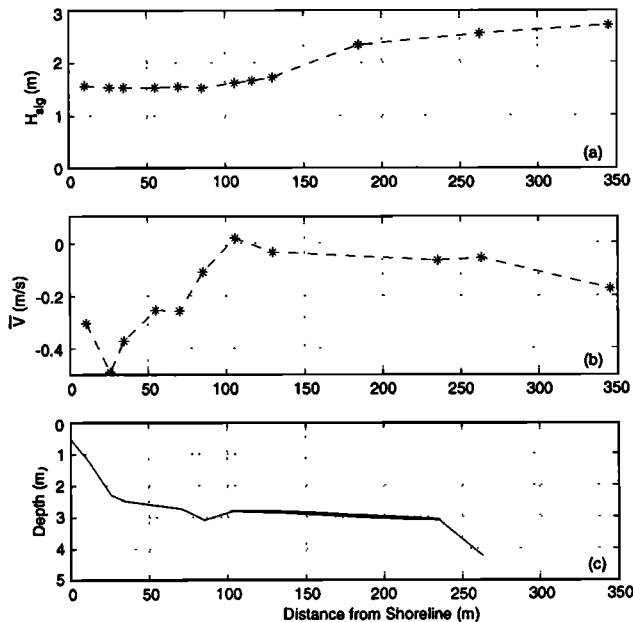


Figure 10. (a) Significant wave height, (b) along-shore current \bar{v} , and (c) depth versus distance from the shoreline observed at 0500 eastern standard time October 16.

personal communication, 1996) suggest the presence of strong alongshore depth variations, and the poststorm (October 18) bathymetry was two-dimensional with a large gap in the sandbar (e.g., Figure 1). The observed alongshore current may have been feeding a rip current visually observed during the storm (E.B. Thornton, personal communication, 1997). In addition, numerical model results with bathymetry similar to that measured on October 18 demonstrate that 2-D effects can be important to the local alongshore momentum balance [Sancho et al., 1995].

5. Summary

The 1-D alongshore momentum balance, with a quadratic parameterization of the bottom stress, integrated from the shoreline to 8-m water depth closes ($r^2 = 0.87$) over a wide range of conditions. The closure suggests that the quadratic form (2) represents well the alongshore bottom stress and that on average the dynamics of the alongshore current are described by the 1-D momentum balance (1). Including the wind forcing statistically improves the integrated-to-8-m-depth momentum balance, demonstrating the importance of wind to nearshore circulation.

A spatially variable drag coefficient c_f statistically improves the integrated-to-8-m-depth momentum balance. The surf zone drag coefficients inferred here are similar to those obtained by Whitford and Thornton [1996] and (for low bed roughness) Garcez Faria et al. [1998]. The cross-shore variation of c_f (0.0033 and 0.0010 within and seaward of the surf zone, re-

spectively) may be associated with increased turbulence from breaking waves inside the surf zone [Church and Thornton, 1993] or cross-shore variations in time-averaged bed roughness [Garcez Faria et al., 1998]. The cross-shore variation of c_f also is consistent with laboratory studies [Cox et al., 1996].

In the surf zone, wind and wave forcing are balanced by the bottom stress. The wind forcing is statistically unimportant within the surf zone relative to the wave forcing but is an $O(1)$ term seaward of the surf zone. The seaward of the surf zone momentum balance between wind forcing and bottom stress does not close as well ($r^2 = 0.36$) as the surf zone momentum balance ($r^2 = 0.79$). Momentum balances on the inner shelf at Duck will be considered in detail elsewhere.

Appendix A: Barotropic Pressure Gradient Estimates

The hourly averaged bottom pressure data acquired with a five-element, 60-km-long array in 6-m water depth centered at the FRF pier [Alessi et al., 1996] was converted to sea surface elevation and demeaned with the 2-month average of each instrument. For each hour, the mean of the five sensors (a spatial mean) was removed, suppressing the large tidal signal with zero phase lag. An empirical orthogonal function decomposition was used to extract the dominant nonzero gradient mode of sea surface elevation from the remaining signal. The first eigenfunction contains 89% percent of the variance and represents a linear tilt in sea surface elevation. The gradient of this first eigenfunction multiplied by its temporal amplitude yields estimates of hourly alongshore sea surface gradients $\partial\eta/\partial y$.

Appendix B: Surf Zone Width (x_b) Estimates

At each pressure sensor along the cross-shore transect the linear energy flux integrated from 0.04 to 0.3 Hz was calculated for each hour assuming shore-normal wave propagation. According to linear theory, on parallel depth contours the energy flux is conserved seaward of x_b , where wave breaking begins. However, measurement errors, inadequacies of linear theory, reflected wave energy, directional spreading, and irregular bathymetry cause considerable scatter in the energy flux estimates. Therefore a heuristic algorithm based on a combination of the decrease in energy flux relative to 8-m water depth, the local energy flux gradient, and time-elapsed video images (R.A. Holman, personal communication, 1996) was used to approximately define the location of the seaward edge of the surf zone x_b . Results that depend on x_b are insensitive to moving all estimates of x_b one sensor closer to shore but, in some cases, vary substantially when the x_b estimates are moved one sensor farther seaward.

Appendix C: Cross-Shore Integration Method

Hourly cross-shore integrals such as

$$\int_{x_1}^{x_2} h\bar{u}dx \quad \int_{x_1}^{x_2} \langle |\bar{u}|v \rangle dx$$

where x_1 and x_2 represent cross-shore instrument locations, were estimated using the trapezoid rule between active sensors. When an instrument at the endpoint (i.e., at $x = x_1$ or $x = x_2$) was inactive, the integral was not computed, with one exception. If the starting point for the integration was the shoreline and the shallowest instrument was inactive, its value was set equal to that of the next offshore sensor. The transect-wide integral to 8-m water depth was estimated for 1176 of the 1440 hour-long records collected during the 2-month experiment. Integrals over the surf zone or the seaward of the surf zone region were estimated only when the outer edge of the surf zone x_b was < 230 m from the shoreline, to ensure sufficient coverage for the seaward of the surf zone integral. The above criteria were satisfied within the surf zone for 858 hours and outside the surf zone for 686 hours. A different current meter (displaced 40 m in the horizontal) was used for the integrations to x_{8m} after October 13, when the 8-m water depth sensor failed. The results are insensitive to which current meter was used when both were active. The degrees of freedom for computing confidence intervals were calculated by dividing the number of hours in the balance by the integral timescale (the time period over which observations are independent [Davis, 1976]). This timescale ranged from 12 to 15 hours, depending on the balance.

Acknowledgments. The array of current meters, sonar altimeters, and pressure sensors was deployed and maintained by staff from the Center for Coastal Studies. Britt Raubenheimer and Edith Gallagher helped collect the data. Excellent logistical support was provided by the U.S. Army Corps of Engineers Field Research Facility. We thank Steve Lentz for providing the wind stress and the alongshore pressure array data, Rob Holman for providing video images, and Ed Thornton for constructive comments. This research was funded by the Office of Naval Research (Coastal Sciences Program) and the National Science Foundation (CooP Program). F.F. received a traineeship from the National Sea Grant College Program, National Oceanic and Atmospheric Administration, U.S. Department of Commerce, under grant NA36RG0537, project R/OE-31 through the California Sea Grant College, and the California State Resources Agency. The views expressed herein are those of the authors and do not necessarily reflect the views of NOAA or any of its subagencies.

References

- Alessi, C.A., S.J. Lentz, and J. Austin, Coastal ocean processes inner-shelf study: Coastal and moored physical oceanographic measurements. *Woods Hole Oceanogr. Inst. Tech. Rep. WHOI-96-6*, 154 pp., Woods Hole Oceanogr. Inst., Woods Hole, Mass., 1996.
- Battjes, J.A., Radiation stresses in short-crested waves, *J. Mar. Res.*, **30**, 56-64, 1972.
- Bowen, A.J., The generation of longshore currents on a plane beach, *J. Mar. Res.*, **27**, 206-215, 1969.
- Church, J.C., and E.B. Thornton, Effects of breaking wave induced turbulence within a longshore current model, *Coastal Eng.*, **20**, 1-28, 1993.
- Cox, D.T., N. Kobayashi, and A. Okayama, Bottom stress in the surf zone, *J. Geophys. Res.*, **101**, 14,337-14,348, 1996.
- Davis, R.E., Predictability of sea surface temperature and sea level pressure anomalies over the North Pacific Ocean, *J. Phys. Oceanogr.*, **6**, 249-266, 1976.
- Dally, W.R., and C.A. Brown, A modeling investigation of the breaking wave roller with application to cross-shore currents, *J. Geophys. Res.*, **100**, 24,873-24,883, 1995.
- Elgar, S., T.H.C. Herbers, and R.T. Guza, Reflection of ocean surface gravity waves from a natural beach, *J. Phys. Oceanogr.*, **24**, 1503-1511, 1994.
- Feddersen, F., R.T. Guza, S. Elgar, and T.H.C. Herbers, Cross-shore structure of longshore currents during Duck94, in *Proc. 25th Int. Coastal Engineering Conf.*, pp. 3666-3679, Am. Soc. of Civ. Eng., New York, 1996.
- Gallagher, E.L., W. Boyd, S. Elgar, R.T. Guza, and B. Woodward, Performance of a sonar altimeter in the nearshore, *Mar. Geol.*, **133**, 241-248, 1996.
- Gallagher, E.L., S. Elgar, and R.T. Guza, Observations of sand bar evolution on a natural beach, *J. Geophys. Res.*, **103**, 3203-3215, 1998.
- Garcez Faria, A.F., E.B. Thornton, T.P. Stanton, C.V. Soares, and T.C. Lippmann, Vertical profiles of longshore currents and related bed shear stress and bottom roughness, *J. Geophys. Res.*, **103**, 3217-3232, 1998.
- Guza, R.T., E.B. Thornton, and N. Christensen Jr., Observations of steady longshore currents in the surf zone, *J. Phys. Oceanogr.*, **16**, 1959-1969, 1986.
- Henderson, F.M., *Open Channel Flow*, Macmillan, Indianapolis, Indiana, 1966.
- Kuik, A.J., G.P. van Vledder, and L.H. Holthuisen, A method for the routine analysis of pitch-and-roll buoy wave data, *J. Phys. Oceanogr.*, **18**, 1020-1034, 1988.
- Large, W.G., and S. Pond, Open ocean momentum flux measurements in moderate to strong winds, *J. Phys. Oceanogr.*, **11**, 324-36, 1981.
- Lentz, S.J., Current dynamics over the northern California inner shelf, *J. Phys. Oceanogr.*, **24**, 2461-2478, 1994.
- Lippmann, T.C., and R.A. Holman, The spatial and temporal variability of sand bar morphology, *J. Geophys. Res.*, **95**, 11,575-11,590, 1990.
- Long, C.E., Index and bulk parameters for frequency-direction spectra measured at CERC Field Research Facility, June 1994 to August 1995, *Misc. Pap. CERC-96-6*, U.S. Army Eng. Waterw. Exp. Stn., Vicksburg, Miss., 1996.
- Longuet-Higgins, M.S., Longshore currents generated by obliquely incident sea waves, 1, *J. Geophys. Res.*, **75**, 6778-6789, 1970.
- Longuet-Higgins, M.S., and R.W. Stewart, Radiation stress in water waves: A physical discussion with application, *Deep Sea Res.*, **11**, 529-563, 1964.
- Mei, C.C., *The Applied Dynamics of Ocean Surface Waves*, World Sci., River Edge, N.J., 1989.
- Putrevu, U., J. Oltman-Shay, and I.A. Svendsen, Effect of alongshore nonuniformities on longshore current predictions, *J. Geophys. Res.*, **100**, 16,119-16,130, 1995.
- Reniers, A., E.B. Thornton, and T.C. Lippmann, Longshore currents over barred beaches. in *Coastal Dynamics '95*, pp. 413-424, Am. Soc. of Civ. Eng., New York, 1995.

- Rennie, S.E., Wind interaction with buoyant plumes on the inner continental shelf, Ph.D. dissertation, 174 pp., Sch. of Mar. Sci., Coll. of William and Mary, Gloucester Point, Va., 1998.
- Rieder, K.F., J.A. Smith, and R.A. Weller, Some evidence of colinear wind stress and wave breaking, *J. Phys. Oceanogr.*, **26**, 2519-2524, 1996.
- Sancho, F.E., I.A. Svendsen, A.R. Van Dongeren, and U. Putrevu, Longshore nonuniformities of nearshore currents, in *Coastal Dynamics '95*, pp. 425-436, Am. Soc. of Civ. Eng., New York, 1995.
- Slinn, D.N., J.S. Allen, P.A. Newberger, and R.A. Holman, Nonlinear shear instabilities of alongshore currents over barred beaches, *J. Geophys. Res.*, in press, 1998.
- Smith, J.M., M. Larson, and N.C. Kraus, Longshore current on a barred beach: Field measurements and calculations, *J. Geophys. Res.*, **98**, 22,717-22,731, 1993.
- Svendsen, I.A., Wave heights and set-up in a surf zone, *Coastal Eng.*, **8**, 303-329, 1984.
- Svendsen, I.A., and U. Putrevu, Nearshore mixing and dispersion, *Proc. R. Soc. London, Ser. A*, **445**, 561-576, 1994.
- Thornton, E.B., Variation of longshore current across the surf zone, in *Proc. 12th Int. Coastal Engineering Conf.*, pp. 291-308, Am. Soc. of Civ. Eng., New York, 1970.
- Thornton, E.B., and R.T. Guza, Transformations of wave height distribution, *J. Geophys. Res.*, **88**, 5925-5938, 1983.
- Thornton, E.B., and R.T. Guza, Surf zone longshore currents and random waves: Field data and models, *J. Phys. Oceanogr.*, **16**, 1165-1178, 1986.
- Whitford, D.J., and E.B. Thornton, Comparison of wind and wave forcing of longshore currents, *Cont. Shelf. Res.*, **13**, 1205-1218, 1993.
- Whitford, D.J., and E.B. Thornton, Bed shear stress coefficients for longshore currents over a barred profile, *Coastal Eng.*, **27**, 243-262, 1996.
-
- S. Elgar, School of Electrical Engineering and Computer Science 2752, Washington State University, Pullman, WA 99164-2752. (e-mail: elgar@eeecs.wsu.edu)
- F. Feddersen and R.T. Guza, Center for Coastal Studies Scripps Institution of Oceanography, University of California, La Jolla, CA 92093-0209. (e-mail: falk@coast.ucsd.edu; rguza@ucsd.edu)
- T.H.C. Herbers, Department of Oceanography, Naval Postgraduate School, Monterey, CA 93943-5122 (e-mail: herbers@zee.oc.nps.navy.mil)

(Received June 18, 1997; revised February 17, 1998; accepted March 24, 1998.)